Muscle synergy patterns as physiological markers of motor cortical damage

Vincent C. K. Cheung[a], Andrea Turolla[b], Michela Agostini[b], Stefano Silvoni[b], Caoimhe Bennis[c], Patrick Kasi[c], Sabrina Paganoni[c], Paolo Bonato[c], and Emilio Bizzi[a,1]

[a]McGovern Institute for Brain Research and Department of Brain and Cognitive Sciences, Massachusetts Institute of Technology, Cambridge, MA 02139; [b]Istituto di Ricovero e Cura a Carattere Scientifico Fondazione Ospedale San Camillo, 30126 Lido di Venezia, Italy; and [c]Department of Physical Medicine and Rehabilitation, Harvard Medical School, Boston, MA 02114

Contributed by Emilio Bizzi, July 16, 2012 (sent for review June 15, 2012)

The experimental findings herein reported are aimed at gaining a perspective on the complex neural events that follow lesions of the motor cortical areas. Cortical damage, whether by trauma or stroke, interferes with the flow of descending signals to the modular interneuronal structures of the spinal cord. These spinal modules subserve normal motor behaviors by activating groups of muscles as individual units (muscle synergies). Damage to the motor cortical areas disrupts the orchestration of the modules, resulting in abnormal movements. To gain insights into this complex process, we recorded myoelectric signals from multiple upper-limb muscles in subjects with cortical lesions. We used a factorization algorithm to identify the muscle synergies. Our factorization analysis revealed, in a quantitative way, three distinct patterns of muscle coordination—including preservation, merging, and fractionation of muscle synergies—that reflect the multiple neural responses that occur after cortical damage. These patterns varied as a function of both the severity of functional impairment and the temporal distance from stroke onset. We think these muscle-synergy patterns can be used as physiological markers of the status of any patient with stroke or trauma, thereby guiding the development of different rehabilitation approaches, as well as future physiological experiments for a further understanding of postinjury mechanisms of motor control and recovery.

motor primitive | electromyography | neurorehabilitation | nonnegative matrix factorization | Virtual Reality Rehabilitation System

There has been considerable experimental evidence suggesting that diverse motor behaviors of vertebrates are constructed by a combination of rudimentary building blocks (motor modules) residing in the spinal cord (1–3). The precise mechanism by which the motor cortical areas preside over the orchestration of these modules for movement generation remains largely unknown. To gain some insight into this question, we studied the muscle activation patterns of stroke survivors with cortical lesions of differing severity. Our goal was to gather data not only for unraveling the complexities emerging after cortical outflow is disrupted, but also for providing a perspective upon which principled rehabilitation strategies could be built.

The utilization of factorization algorithms for analyzing muscle activity recorded during motor behaviors has made it possible to decompose myoelectric activation patterns into their building blocks, thereby revealing the modular architecture of the motor system. In the last few years, we and others (2, 3) have pursued this approach to shed light on old questions such as how the motor system circumvents the need to control its large number of degrees of freedom (4) through a flexible combination of motor modules in both animals and humans. Other investigators have used factorization analysis to gain a new understanding of spinal cord functions (5–8), of postural control (9, 10), and of motor development (11, 12).

The factorization analysis that we and others have used models motor modules as groups of muscles activated together (muscle synergies). Each muscle synergy represents a time-invariant profile of activation across muscles, activated by a time-varying coefficient. When individual synergies, scaled by their coefficients, are summed together, the muscle activation patterns, recorded during movements as electromyographic signals (EMGs), are faithfully reconstructed (Fig. 1).

In this report, we focus on upper-limb muscle synergies of a group of patients with stroke ($n = 31$) with a wide range of unilateral motor impairment (Table S1). To identify muscle synergies, we recorded EMG patterns from both arms during a variety of tasks and reaching movements. We used the nonnegative matrix factorization (NMF) algorithm (13) to extract from the EMGs the number of muscle synergies necessary for an 80% R^2 EMG reconstruction and then compared the synergies of the two arms. Our analysis revealed three distinct patterns of muscle synergies, reflecting preservation, merging, and fractionation of the unaffected-arm muscle synergies in the stroke-affected arm, respectively. These patterns manifested themselves to varying degrees in different patient groups, suggesting that they may be used as markers of the physiological status of stroke survivors.

Results

In mildly impaired patients recorded shortly after stroke, we observed that the muscle synergies of the stroke-affected arm were strikingly similar to those of the unaffected arm despite marked differences in motor performance between the arms. For example, in one such patient with an upper-arm Fugl–Meyer (FM) score of 50 (of a maximum score of 66) recorded 2.1 mo poststroke, each of the seven muscle synergies of the affected arm (Fig. 2*A*, red) could be matched to an unaffected-arm synergy (blue) with a scalar-product similarity of 0.93 ± 0.03 (mean ± SD). This observation is not only consistent with the conclusion we reached in an earlier study (14), but also compatible with the proposal that muscle synergies are structured in the spinal cord, and after cortical stroke, altered descending commands from supraspinal areas generate abnormal motor behaviors through faulty activations of the spinal modules (14, 15) (see Fig. S4).

In contrast, in subjects with severe motor impairment (FM score ≤30), regardless of when the patients were recorded relative to stroke onset, there was much less resemblance between the synergies of the two arms. In the example shown in Fig. 2*B*, the four synergies extracted from the affected arm (red) could reconstruct the EMG patterns recorded during voluntary movement as effectively as the six synergies extracted from the unaffected arm (blue). This difference in data dimensionality suggests

Author contributions: V.C.K.C., P.B., and E.B. designed research; V.C.K.C., A.T., M.A., S.S., C.B., P.K., and S.P. performed research; V.C.K.C. analyzed data; and V.C.K.C. and E.B. wrote the paper.

The authors declare no conflict of interest.

[1]To whom correspondence should be addressed. E-mail: ebizzi@mit.edu.

This article contains supporting information online at www.pnas.org/lookup/suppl/doi:10.1073/pnas.1212056109/-/DCSupplemental.

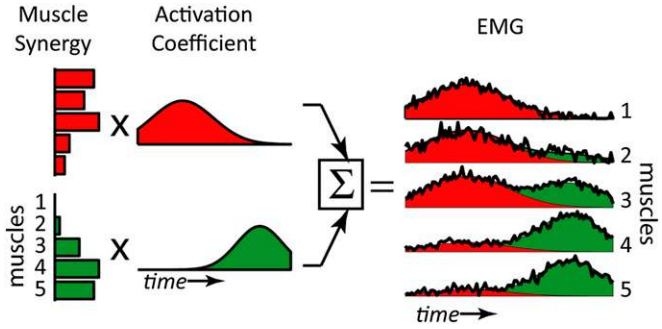

Fig. 1. A schematic illustrating how muscle synergies are linearly combined to generate muscle patterns recorded as electromyographic signals (EMGs). Each of the two muscle synergies shown (red and green bars) is represented as an activation balance profile across muscles (muscles 1–5) and activated, through multiplication, by a time-dependent coefficient. The EMG waveforms resulting from the activations of individual synergies are then summed together to reconstruct the recorded EMGs (black lines). In the schematic, each color in the EMG reconstruction reflects how the waveforms from the synergy coded by the same color contribute to the reconstruction.

that the apparent dissimilarity between the synergies of the two arms may be attributed to a merging of the synergies that were present before stroke in the impaired limb, a merging that persisted throughout the movement trials. We thus proceeded to investigate this merging systematically with a computational procedure that automatically searched, among the unaffected-arm synergies, those that could be linearly combined to reconstruct each affected-arm synergy (*SI Materials and Methods*). In Fig. 3*A*, the four synergies *A1*–*A4* extracted from the affected-arm EMGs (red) were reconstructed by linearly combining two to three synergies from the unaffected arm (blue). Synergy *A1*, for instance, was explained as a combination of *U1* and *U5*; synergy *A2*, of *U2* and *U5*; and so on. The scalar-product similarity between the extracted (red) and reconstructed (pink) synergies for the stroke-affected arm (0.92 ± 0.03) was indeed much higher than the values obtained either by directly matching the synergies of the two arms ($P < 0.03$; 0.78 ± 0.09) (Fig. 2*B*) or by performing this merging analysis with random unaffected-arm synergies ($P < 10^{-4}$; 0.81 ± 0.02) (Fig. S1).

We applied this merging analysis to the muscle synergies of all other patients and quantified the degree of synergy merging in each patient by calculating the mean number of unaffected-arm synergies found to merge into each affected-arm synergy (thus, in the above example, this number is the average of 2, 2, 3, and 3, corresponding to the numbers for synergies *A1*–*A4*, respectively, which equals 2.5; a value of 1 corresponds to an absence of merging). We found that this index of synergy merging correlated negatively, and significantly, with the patients' FM scores

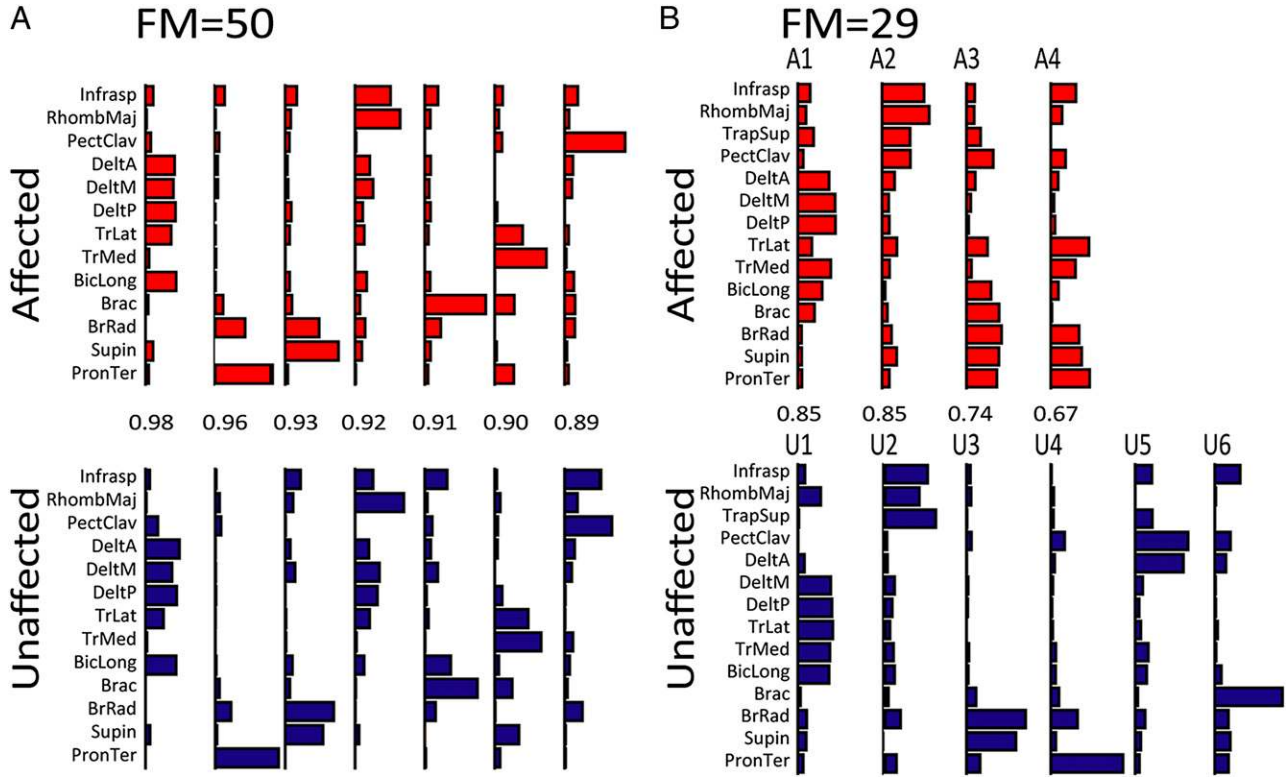

Fig. 2. Preservation of muscle synergies in a mildly impaired patient with stroke but not in a severely impaired patient. (*A*) The muscle synergies extracted from the EMGs of the stroke-affected (red) and unaffected (blue) arms of a mildly impaired patient with stroke with a Fugl–Meyer (FM) score of 50. For both arms, seven muscle synergies were sufficient for an EMG reconstruction R^2 of ~80%. Each affected-arm synergy was matched to an unaffected-arm synergy giving the highest scalar-product similarity value, shown in between each synergy pair. All seven pairs had high similarity values (0.89–0.98), suggesting preservation of the normal muscle synergies in the stroke-affected arm of this patient. (*B*) The muscle synergies of a severely impaired stroke patient with FM score of 29. For this subject only four synergies were needed for reconstructing the affected-arm EMGs (synergies *A1*–*A4*) whereas six were needed for the unaffected arm (synergies *U1*–*U6*). The similarity values between the synergies of the two arms were lower (0.67–0.85), but the affected-arm synergies tended to have activation components in more muscles than the unaffected-arm synergies (e.g., compare *A3* with *U3* and *A4* with *U4*). This observation suggests that the apparent dissimilarity between the synergies of the two arms may be due to merging of the unaffected-arm synergies in the stroke-affected arm. Infrasp, infraspinatus; RhombMaj, rhomboid major; TrapSup, trapezius superior; PectClav, clavicular head of pectoralis major; DeltA, anterior part of deltoid; DeltM, medial part of deltoid; DeltP, posterior part of deltoid; TrLat, lateral head of triceps brachii; TrMed, medial head of triceps brachii; BicLong, long head of biceps brachii; Brac, brachialis; BrRad, brachioradialis; Supin, supinator; PronTer, pronator teres.

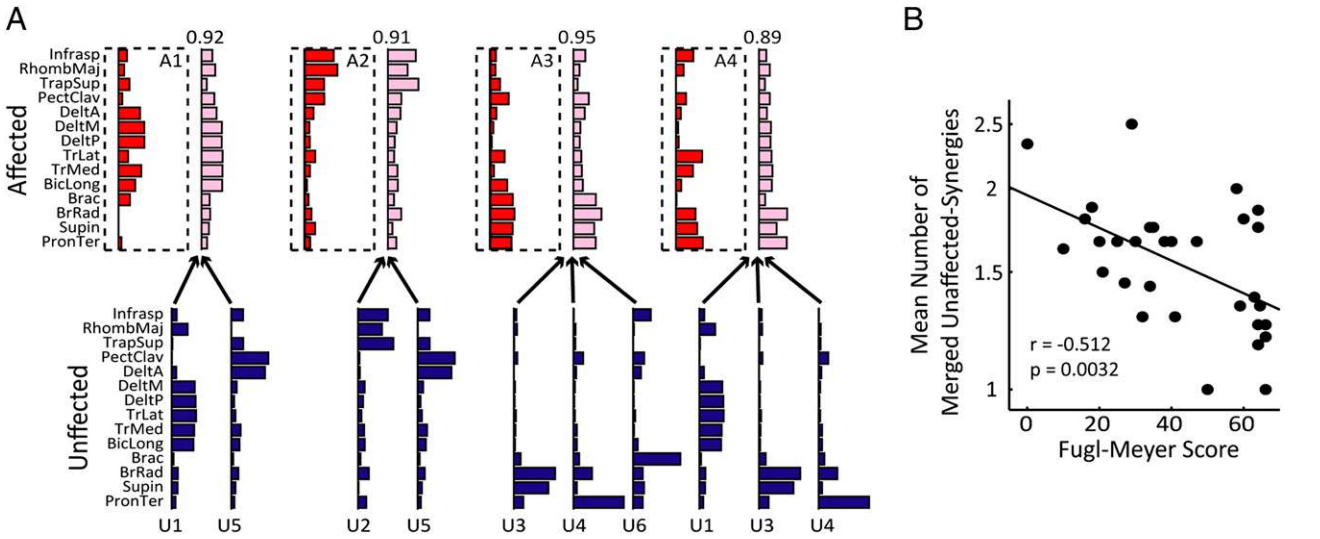

Fig. 3. The stroke-affected arm muscle synergies of severely impaired patients explained as merging of unaffected-arm synergies. (*A*) We devised a computational procedure that systematically finds the subset of unaffected-arm synergies that can be linearly combined to reconstruct each affected-arm muscle synergy. Each affected-arm synergy from the example shown in Fig. 2*B* (red, *A1*–*A4*) was reconstructed by merging two to three unaffected-arm synergies (blue, *U1*–*U6*). Synergy *A1*, for instance, could be reconstructed by combining *U1* and *U5*; synergy *A2*, by combining *U2* and *U5*; and so on. The reconstructed affected-arm synergies (pink), when compared with the synergies extracted from the affected-arm EMGs (red), yielded high similarity values (0.89–0.95, shown between each extracted and reconstructed synergy pair for the affected arm). (*B*) We derived an index quantifying the degree of synergy merging by calculating the mean number of unaffected-arm synergies found merging into each affected-arm synergy. When calculating this average, we included in our statistic only those affected-arm synergies that could be well reconstructed as a combination of unaffected-arm synergies (scalar product >0.75). Across all patients ($n = 31$), we found a significant, negative correlation between our index of synergy merging (in log scale) and the FM score ($r = -0.512$, $P = 0.0032$). Thus, the more impaired the patient with stroke, the more likely that an affected-arm synergy represents a merging of multiple unaffected-arm synergies.

(Fig. 3*B*; $r = -0.51$, $P < 0.01$); thus, the more severe the impairment, the more likely it is that an affected-arm synergy represents a merging of multiple unaffected synergies. Further statistical tests confirmed that the degree of merging of unaffected-arm synergies varied with the FM score [three-way ANOVA, $F(1, 30) = 8.0$, $P < 0.01$], but not with poststroke duration ($F = 0.01$, $P > 0.9$) or with the side affected by the stroke ($F = 0.90$, $P > 0.3$) (Fig. S2).

Whereas our model of synergy merging has enabled us to reconstruct the affected-arm muscle synergies in most patients with good fidelity, in some subjects, particularly the chronic survivors, there was a portion of affected-arm synergies that could not be well explained by any combination of merging (Fig. 4*A* and Fig. S3). For instance, in one chronic stroke survivor (poststroke duration of 450.7 mo), whereas one of the six synergies extracted from the affected-arm EMGs could be very well reconstructed (Fig. 4*B*, synergy *A1*; scalar product of 0.91), the rest could be only moderately well or poorly reconstructed (*A2*–*A6*; scalar product of 0.71–0.81). It occurred to us that the affected-arm synergies that could not be explained as a merging were in fact fractionations of unaffected-arm synergies. Using a computational procedure, we identified affected-arm synergies *A2* and *A3* as fractionations of one unaffected-arm synergy (Fig. 4*C*, *U1*) and *A4*, *A5*, and *A6* as fractionations of another (*U3*).

In 18 of the 31 subjects, our procedure identified two or more synergies for the impaired arm as fractionations of one or multiple unaffected-arm synergies. Within this group of subjects, the percentage of affected-arm synergies found to be fractionations correlated strongly with poststroke duration (Fig. 4*D*; $r = 0.66$, $P < 0.004$).

Discussion

The muscle synergies extracted by the factorization algorithm from the EMGs of multiple tasks (Figs. 2–4) have allowed us to reveal, in a quantitative way, distinct myographic patterns reflecting the physiological processes that occur following cortical damage. These patterns vary as a function of both the severity of motor impairment and the temporal distance from stroke onset. Whether they also depend on the anatomical location of the lesion would require further analysis of the magnetic resonance imaging data of our subjects.

In our analysis, we have compared the muscle synergies of the stroke-affected arm with those of the unaffected arm of the same subject. The patterns of muscle synergies we have revealed rely on the assumption that the unaffected-arm synergies are themselves not changed by either the stroke lesions or the elapse of time after stroke. This assumption is supported by an earlier observation that the unaffected-arm synergies in patients with stroke are similar to the ones identified in the arms of healthy control subjects (14).

Central to the present investigation is the use of a factorization algorithm (NMF) to extract muscle synergies from the EMGs of multiple muscles. The factorization procedure essentially performs a dimensionality reduction by grouping the muscles that tend to covary in the dataset into individual synergies (Fig. 1). The set of extracted muscle synergies may thus be viewed as a compact representation of the most salient features embedded within the variability present in the EMG dataset. The use of an algorithm provides an objective and efficient means to identify, from large, high-dimensional EMG data recorded from multiple tasks, basic muscle groupings that are not necessarily obvious from visual inspection of the raw data or simple correlation analysis between the EMGs of muscle pairs. Importantly, an earlier study has shown that different linear factorization algorithms (except principal component analysis) produced similar synergies in both simulated and experimental datasets (16). This result supports that the extracted synergies are likely not artifacts contingent upon the assumptions of NMF, but reflect structures of the motor modules used by the motor system for movement control.

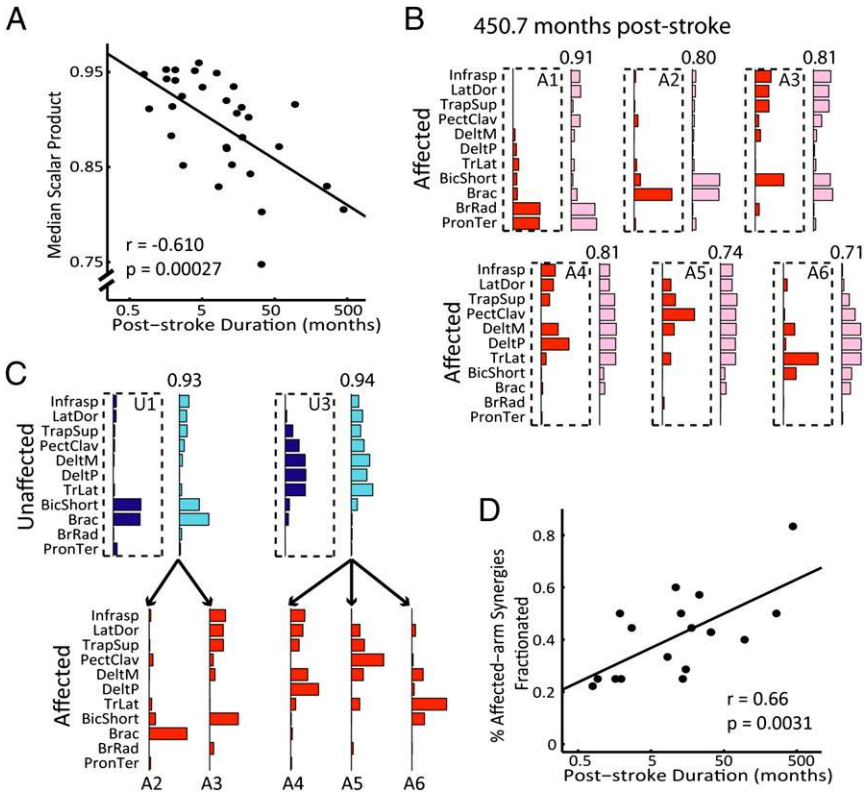

Fig. 4. The stroke-affected arm muscle synergies of chronic patients explained as fractionations of unaffected-arm synergies. (*A*) Some of the affected-arm synergies from the chronic patients in our dataset could neither be directly matched to an unaffected-arm synergy nor be explained as a merging of multiple unaffected-arm synergies. In fact, the median scalar-product similarity value between the extracted and reconstructed (via the merging model) affected-arm synergies decreased with the subjects' poststroke duration (in log scale) ($r = -0.610$, $P = 2.7 \times 10^{-4}$). (*B*) The muscle synergies of a very chronic patient (poststroke duration = 450.7 mo) extracted from the affected-arm EMGs (red, *A1–A6*) and their corresponding reconstructions by merging unaffected-arm synergies (pink). Of these six synergies, only one could be well reconstructed (*A1*). (*C*) The affected-arm synergies that could not be well reconstructed by the merging model in *B* (*A2–A6*) could instead be explained as fractionations of unaffected-arm synergies. Our computational procedure identified synergies *A2* and *A3* to be fractionations of synergy *U1* for the unaffected arm, and *A4–A6* as fractionations of synergy *U3*. The affected-arm synergies identified as fractionations (red) could in fact be linearly combined to result in reconstructions of their corresponding unaffected-arm synergies (cyan) that matched very well to the synergies extracted from the unaffected-arm EMGs (blue) (scalar product = 0.93–0.94). (*D*) Within the group of subjects in whose affected-arm synergies fractionations were observed ($n = 18$), the percentage of affected-arm synergies identified to be fractionations of unaffected-arm synergies increased with the subjects' poststroke duration (in log scale) ($r = 0.66$, $P = 0.0031$).

Our factorization procedure has identified three basic patterns of muscle synergies. In cases of mild-to-moderate impairment (FM > 30), we observed that the synergies in the affected and unaffected arms were similar even though the muscle activation patterns were different (Fig. 2*A*). This observation indicates that the output of spinal modules can still be retrieved by the factorization procedure. However, as reflected by the differences in the activation coefficients of these preserved synergies between the two arms (Fig. S4), the machinery for activating synergies, presumably under cortical control, has faltered after stroke. It is the failure of activating the synergies in a correct way that generates abnormal motor behaviors.

In cases of severe impairment (FM ≤ 30), we observed a different pattern of muscle synergies. In the affected arm, multiple synergies appeared to merge (Fig. 2*B*). As a consequence of this merging, the EMGs of the affected arm could be reconstructed with fewer synergies (Fig. S5). This merging of muscle synergies we observed is compatible with the poststroke "cocontractions" of muscles described in the literature (17–20) and a previous report of motor-module fusion in the affected lower limb of stroke survivors (21). In fact, in our data certain combinations of muscle synergies were observed to merge more frequently than others across patients (Fig. S6). The merging of these specific muscle synergies could potentially account for the previously observed poststroke couplings of shoulder and elbow actions (22), which could in turn lead to a reduction in the range of joint motion.

Whereas the former two patterns are related to the severity of motor impairment, the third pattern we identified emerged only after years from the initial injury. In a subset of patients with chronic stroke, a portion of the synergies in the affected arm appeared to be fractionations of the synergies observed in the unaffected arm (Fig. 4*C*), and this fractionation process tended to increase the number of synergies required for adequate description of the affected-arm EMGs (Fig. S5). It remains to be verified whether fractionation is an adaptive process triggered in response to the poststroke motor impairment. For instance, an increased flexibility of controlling the shoulder and upper-arm muscles provided by synergy fractionation could compensate for impaired motions of the more distal joints resulting from stroke (17).

Even though we present here the preservation, merging, and fractionation of muscle synergies as three distinct poststroke responses, we note that two or all three of these responses could be present simultaneously in the same subject (Fig. S7). The extent to which each of these three responses manifests itself in the stroke-affected arm could therefore serve as a precise and quantifiable marker of the physiological status of the patient at any given time.

At this point it would be hazardous to speculate upon the neural mechanisms underlying both merging and fractionation of

muscle synergies. The motor system is a complex, integrated system with ascending and descending pathways working in ways that defy simple hierarchical descriptions. Even though the lesions are cortical, the merging and fractionation might be dependent on either neural changes at the cortical level (23) or other processes at the brainstem or spinal cord levels unmasked by the cortical lesions (17). Although it is premature to advance any concrete hypothesis on the origin of these three patterns of muscle synergy, we believe a description of these patterns is nonetheless important because the patterns provide physiological markers that can be used for shedding light on the complex processes that follow accidents involving the cortical motor system.

With animal models, the use of these markers, in conjunction with conventional physiological and behavioral techniques, may provide an understanding of how cortical and subcortical processes interact to produce the motor patterns observed in patients with stroke. A more challenging task, however, is to develop more effective rehabilitation procedures on the basis of the data provided by our factorization analysis. At the very least, the observation of merging and fractionation of muscle synergies should prompt the development of different therapeutic approaches. In the long run, the markers we have identified might be profitably used for assessing the efficacy of any existing or new rehabilitation therapies by providing physiological information on how they affect the dynamics of motor recovery from cortical lesions. Finally, these markers may represent a step toward the establishment of customized therapies tailored to the conditions of individual patients.

Materials and Methods

Subjects. Thirty-one stroke survivors were recruited from the San Camillo Hospital, Lido di Venezia, Italy (n = 21) and the Spaulding Rehabilitation Hospital, Boston (n = 10). All patients studied suffered from a mostly unilateral cortical and subcortical lesion resulting from either an ischemic or a hemorrhagic stroke (Table S1). All procedures were approved by the Ethics Committees of the San Camillo Hospital, Spaulding Rehabilitation Hospital, and Massachusetts Institute of Technology. All participants gave informed consent before experimentations.

Behavioral Tasks and EMG Recordings. Each subject was asked to perform multiple upper-limb tasks with each of the two arms so that the muscle patterns from the stroke-affected arm could be compared with those from the unaffected arm of the same subject. At San Camillo, the motor behaviors tested consisted of seven virtual-reality tasks (10–11 trials per task). At Spaulding, subjects were asked to perform a point-to-point reaching task consisting of ballistic movements from an initial position to 1 of 12 possible targets in 3D space, and then from the target back to the initial position (3–4 trials per target). As the subject performed the tasks, EMG activities of 10–16 shoulder, upper-arm, and forearm muscles of each arm were collected using surface bipolar electrodes.

Extracting Muscle Synergies. Muscle synergies were extracted from filtered, rectified, integrated, and variance-normalized EMGs of each arm of each subject using the NMF algorithm (13). The NMF models the activities of the recorded muscles as a linear combination of time-invariant muscle synergies, each activated by a time-varying activation coefficient (Fig. 1). To identify the number of muscle synergies composing the EMGs, we successively increased the number of synergies extracted from one to the number of muscles recorded and selected the minimum number of synergies required for a cross-validated EMG-reconstruction R^2 of 80%. Because the synergies and their coefficients extracted from the data may represent a local extremum on the R^2 surface, we repeated the synergy extraction 50 times and selected the solution giving the highest R^2 for further analyses.

Merging and Fractionation of Muscle Synergies. We investigated whether the observed muscle synergies in the stroke-affected arm could be explained as multiple synergies merging together by modeling each affected-arm synergy as a linear combination of the set of unaffected-arm synergies. The coefficients of this linear combination were identified through a standard nonnegative least-squares procedure (*SI Materials and Methods*). For every affected-arm synergy, an unaffected-arm synergy was defined to contribute to the merging if its associated coefficient was >0.2. Note that in this model, each unaffected-arm synergy could contribute to the merging of more than one affected-arm synergy.

In addition, we investigated whether two or more affected-arm synergies could be fractionations of any unaffected-arm synergy by modeling each unaffected-arm synergy as a linear combination of the set of affected-arm synergies. Thus, the fractionation model is equivalent to the one obtained by swapping the roles of the unaffected- and affected-arm synergies in the merging model. Because each affected-arm synergy could not simultaneously be fractionations of more than one unaffected-arm synergy, we imposed the additional constraint in the least-squares optimization that each affected-arm synergy could contribute to the reconstruction of at most one unaffected-arm synergy.

ACKNOWLEDGMENTS. We thank Clara Genna of the San Camillo Hospital and Andrea Valsecchi, Giacomo Severini, and Martina Coscia of the Spaulding Rehabilitation Hospital for assistance in data collection, and Charlotte Potak and Ellen Connors for administrative assistance. This work was funded by National Institutes of Health Grant RC1-NS068103-01 (to E.B.) and Italian Ministry of Health Grant ART56-NMC-704763 (to A.T., M.A., and S.S.).

1. Flash T, Hochner B (2005) Motor primitives in vertebrates and invertebrates. *Curr Opin Neurobiol* 15:660–666.
2. Bizzi E, Cheung VCK, d'Avella A, Saltiel P, Tresch MC (2008) Combining modules for movement. *Brain Res Brain Res Rev* 57:125–133.
3. Tresch MC, Saltiel P, d'Avella A, Bizzi E (2002) Coordination and localization in spinal motor systems. *Brain Res Brain Res Rev* 40:66–79.
4. Bernstein NA (1967) *The Co-ordination and Regulation of Movements* (Pergamon, Oxford).
5. Tresch MC, Saltiel P, Bizzi E (1999) The construction of movement by the spinal cord. *Nat Neurosci* 2:162–167.
6. Saltiel P, Wyler-Duda K, d'Avella A, Ajemian RJ, Bizzi E (2005) Localization and connectivity in spinal interneuronal networks: The adduction-caudal extension-flexion rhythm in the frog. *J Neurophysiol* 94:2120–2138.
7. Hart CB, Giszter SF (2010) A neural basis for motor primitives in the spinal cord. *J Neurosci* 30:1322–1336.
8. Roh J, Cheung VCK, Bizzi E (2011) Modules in the brain stem and spinal cord underlying motor behaviors. *J Neurophysiol* 106:1363–1378.
9. Ting LH, Macpherson JM (2005) A limited set of muscle synergies for force control during a postural task. *J Neurophysiol* 93:609–613.
10. Torres-Oviedo G, Ting LH (2010) Subject-specific muscle synergies in human balance control are consistent across different biomechanical contexts. *J Neurophysiol* 103: 3084–3098.
11. Monaco V, Ghionzoli A, Micera S (2010) Age-related modifications of muscle synergies and spinal cord activity during locomotion. *J Neurophysiol* 104:2092–2102.
12. Dominici N, et al. (2011) Locomotor primitives in newborn babies and their development. *Science* 334:997–999.
13. Lee DD, Seung HS (1999) Learning the parts of objects by non-negative matrix factorization. *Nature* 401:788–791.
14. Cheung VCK, et al. (2009) Stability of muscle synergies for voluntary actions after cortical stroke in humans. *Proc Natl Acad Sci USA* 106:19563–19568.
15. Yakovenko S, Krouchev N, Drew T (2011) Sequential activation of motor cortical neurons contributes to intralimb coordination during reaching in the cat by modulating muscle synergies. *J Neurophysiol* 105:388–409.
16. Tresch MC, Cheung VCK, d'Avella A (2006) Matrix factorization algorithms for the identification of muscle synergies: Evaluation on simulated and experimental data sets. *J Neurophysiol* 95:2199–2212.
17. Dewald JPA, Pope PS, Given JD, Buchanan TS, Rymer WZ (1995) Abnormal muscle coactivation patterns during isometric torque generation at the elbow and shoulder in hemiparetic subjects. *Brain* 118:495–510.
18. Beer RF, Given JD, Dewald JPA (1999) Task-dependent weakness at the elbow in patients with hemiparesis. *Arch Phys Med Rehabil* 80:766–772.
19. Neckel N, Pelliccio M, Nichols D, Hidler J (2006) Quantification of functional weakness and abnormal synergy patterns in the lower limb of individuals with chronic stroke. *J Neuroeng Rehabil* 3:17.
20. Marciniak C (2011) Poststroke hypertonicity: Upper limb assessment and treatment. *Top Stroke Rehabil* 18:179–194.
21. Clark DJ, Ting LH, Zajac FE, Neptune RR, Kautz SA (2010) Merging of healthy motor modules predicts reduced locomotor performance and muscle coordination complexity post-stroke. *J Neurophysiol* 103:844–857.
22. Brunnstrom S (1970) *Movement Therapy in Hemiplegia* (Harper & Row, New York).
23. Yao J, Chen A, Carmona C, Dewald JPA (2009) Cortical overlap of joint representations contributes to the loss of independent joint control following stroke. *Neuroimage* 45:490–499.

Supporting Information

Cheung et al. 10.1073/pnas.1212056109

SI Materials and Methods

Subjects. A total of 31 stroke survivors (mean age = 61.6) were recruited from the San Camillo Hospital, Lido di Venezia, Italy (n = 21) and the Spaulding Rehabilitation Hospital, Boston (n = 10). All patients studied suffered from a mostly unilateral cortical and subcortical lesion resulting from either an ischemic or a hemorrhagic stroke (Table S1). The location and extent of the lesion were obtained from radiological interpretations of the patients' magnetic resonance imaging records. The residual motor functions of the patients' stroke-affected arm were quantified using the upper-extremity Fugl–Meyer scale (maximum score of 66). Data from 8 of the San Camillo patients have been previously described (1).

All subjects studied had received various amounts of physical rehabilitation therapy before recording. For the San Camillo patients, the treatments administered included both standard physical therapy and upper-limb exercises performed on the Virtual Reality Rehabilitation System (VRRS) (Khymeia).

All procedures were approved by the Ethics Committee of the San Camillo Hospital, the Human Studies Committee of the Spaulding Rehabilitation Hospital, and the Committee on the Use of Humans as Experimental Subjects of Massachusetts Institute of Technology. All participants gave informed consent before experimentation.

Behavioral Tasks. Each subject was asked to perform multiple upper-limb tasks with each of the two arms so that the muscle patterns from the stroke-affected arm could be compared with those from the unaffected arm of the same subject. At the San Camillo Hospital, the motor behaviors tested consisted of seven virtual-reality tasks (10–11 trials per task) designed for eliciting adequate variability of shoulder and elbow motions, necessary for the identification of muscle synergies, with a reasonable number of movement trials. They included simple upward reaching, shoulder abduction, forward reaching across a single spatial constraint, upward reaching across two spatial constraints, hand pronation, shoulder circumduction, and moving the hand along a path together with forearm pronation. The tasks required for both arms were identical, except that their trajectories were mirror images of each other.

At the Spaulding Rehabilitation Hospital, motion variability was elicited with a similar point-to-point reaching task consisting of ballistic movements from an initial position to 1 of 12 possible targets in three-dimensional space, and then from the target back to the initial position. Target locations were specified by equally spaced points along the circumference of a circular wooden panel (radius of 20.5 cm) placed in front of a sitting subject. The position of the panel was adjusted so that its center aligned both vertically and mediolaterally with the shoulder of the recorded arm, and the distance between the panel's center and the shoulder equaled the shoulder-to-hand length of the fully extended unaffected arm. The initial starting position for each reach was indicated by a marker attached to the end of a metal stick mounted on a frame placed in front of the panel, so that the starting point was at the height of the panel's center and the distance between them equaled the forearm's length measured from ulnar to lateral epicondyle of the unaffected arm. For each trial, the subject was instructed to move from the initial position to the target and then from the target back to the initial position. For each of the two arms, three to four blocks of trials were performed. Each block consisted of 12 trials (1 trial per target), and the within-block ordering of targets was randomized each time.

Electromyographic (EMG) Recordings and Preprocessing. As the subject performed the behavioral tasks, EMG activities of 10–16 shoulder, upper-arm, and forearm muscles of each arm were collected at 1,000 Hz (San Camillo) or 3,000 Hz (Spaulding), using surface bipolar electrodes (San Camillo, Biopac Systems; Spaulding, MA-300; Motion Lab Systems). The muscles recorded included infraspinatus; teres major (at San Camillo only); latissimus dorsi (at Spaulding only); rhomboid major; superior trapezius; pectoralis major, clavicular head; deltoid, anterior, medial, and posterior parts; triceps brachii, lateral head; triceps brachii, medial head (San Camillo only); biceps brachii, short and long heads; brachialis; brachioradialis; supinator (San Camillo only); and pronator teres. Before electrode placement, the skin surface where the electrodes would be positioned was cleaned with alcohol wipes, and any excess body hair on the surface was shaved. Placement positions were identified according to guidelines of the Surface Electromyography for the Non-Invasive Assessment of Muscles–European Community Project (SENIAM) and Delagi et al. (2). All EMGs collected were stored in a computer and subsequently analyzed offline, using customized functions written in Matlab (Mathworks).

Before muscle synergy analysis, the collected EMGs were preprocessed as described before (1). Briefly, the EMGs were first high-pass filtered (window-based finite impulse response filter, 50th order, cutoff of 50 Hz), then rectified, and then low-pass filtered (window-based finite impulse response filter, 50th order, cutoff of 20 Hz), and finally integrated over 20-ms intervals. Data of every trial were carefully inspected before extraction of synergies to ensure that none of the trials contained high-amplitude spikes arising from noise. To equalize EMG-amplitude differences between muscles so that subsequent extractions of synergies from the EMGs would not be biased into describing only the high-amplitude muscles, the data from each muscle of each arm were normalized to unit variance (3, 4).

Extracting Muscle Synergies. As in previous studies (5, 6), muscle synergies were extracted from the EMGs of all tasks from each arm of each subject using the nonnegative matrix factorization (NMF) algorithm (7), which models the activities of the recorded muscles as a linear combination of time-invariant muscle synergies, each activated by a time-varying activation coefficient (Fig. 1). This model may be mathematically expressed as

$$\vec{D}(t) = \sum_{i=1}^{N} c_i(t)\vec{w}_i + \vec{\varepsilon}, \qquad \text{[S1]}$$

where $\vec{D}(t)$ is the vector of EMG activities collected at time t, N is the number of muscle synergies extracted, $\vec{w}_i$ is a time-invariant nonnegative vector in muscle space denoting the ith muscle synergy, $c_i(t)$ is the nonnegative activation coefficient for the ith synergy, and $\vec{\varepsilon}$ is any residual activities unexplained by the linear combination. For any prespecified N, the NMF finds from the EMGs both $c_i(t)$ and $\vec{w}_i$ by minimizing $\vec{\varepsilon}$, with the additional assumption that $\vec{\varepsilon}$ follows a Gaussian distribution (8). In our NMF implementation, the algorithm was initialized with random synergy and coefficient matrices whose elements were drawn from a uniform distribution between 0 and 1; values of these matrices were then iteratively updated until convergence, defined as having 20 consecutive iterations that resulted in a change of EMG-reconstruction $R^2 < 0.01\%$. Because the solutions for the synergies and their coefficients found by the algorithm may represent a local extremum on the R^2 surface, we repeated the synergy extraction 50 times for every arm of every

subject and selected the synergies from the run giving the highest R^2 for further analyses.

To identify the number of muscle synergies composing the EMGs (N in Eq. **S1**), we successively increased the number of synergies extracted from one to the number of muscles recorded and selected the minimum number of synergies required for an EMG reconstruction R^2 of 80%. More precisely, the R^2 values we used for this step were cross-validated values obtained by first extracting synergies from a randomly selected half of the episodes (the training subset), and then fitting the extracted synergies to the other unused half (the testing subset). We calculated R^2 values for individual EMG trials in the testing subset (instead of one R^2 value for all episodes in the testing subset), allowing us to derive, from this distribution of R^2 values, a 90% confidence interval for the mean reconstruction R^2 for the individual testing EMG trials. This cross-validation was repeated 10 times, each time with different randomly selected training and testing subsets. A plot of the confidence-interval upper bound, averaged across the 10 cross-validations, against the number of synergies extracted then enabled us to select the minimum number of synergies required for an 80% R^2 reconstruction.

Model of Synergy Merging. When we inspected the synergies extracted from the EMGs of the severely impaired stroke patients, we noticed consistently that the structures of many synergies for the stroke-affected arm were less sparse (i.e., there were more muscle components within each synergy) than those for the unaffected arm. Detailed visual examinations of the synergy sets of the two arms further suggested to us that some of the affected-arm synergies may result from merging of multiple unaffected-arm synergies, similar to what Clark et al. (9) have previously observed for lower-limb synergies in stroke survivors. These observations prompted us to derive a computational method for systematically identifying how the unaffected-arm synergies merged together in the synergy set of the affected arm. For this identification, we modeled each affected-arm synergy as a linear combination of the unaffected-arm synergies,

$$\vec{w}_i^{\,a} \approx \sum_{k=1}^{N^u} m_k^i \vec{w}_k^{\,u}, \quad m_k^i \geq 0, \quad i = 1...N^a, \qquad \textbf{[S2]}$$

where $\vec{w}_i^{\,a}$ is the ith affected-arm synergy, $\vec{w}_k^{\,u}$ is the kth unaffected-arm synergy, N^u is the number of unaffected-arm synergies extracted, N^a is the number of affected-arm synergies extracted, and m_k^i is a nonnegative coefficient denoting the degree of contribution of the kth unaffected-arm synergy to the structure of the ith affected-arm synergy in the linear combination. Note that in this model, each unaffected-arm synergy could contribute to more than one affected-arm synergy. For every affected-arm synergy, an unaffected-arm synergy was defined to contribute to the merging if its associated merging coefficient was >0.2.

Identification of the merging coefficients $\vec{m}^i$ was achieved using nonnegative least squares implemented through the lsqnonneg function of Matlab (optimization toolbox). This identification amounts to projecting each $\vec{w}_i^{\,a}$ onto the space spanned by $\{\vec{w}_1^{\,u}, \vec{w}_2^{\,u}, ..., \vec{w}_{N^u}^{\,u}\}$. Similarity between the original affected-arm synergy and that reconstructed from combination of unaffected-arm synergies was measured by the scalar product between them (after normalization to unit vectors).

Model of Synergy Fractionation. When the above model of synergy merging was applied to the synergy sets extracted from EMGs of the impaired arm, we noticed that some affected-arm synergies could not be well reconstructed by any combination of unaffected-arm synergies (scalar product <0.75). These synergies, on the other hand, often contained activations in subsets of muscles present in another unaffected-arm synergy and thus appeared to be split-off fractionations of a muscle synergy of the unaffected arm. This observation prompted us to systematically identify the affected-arm synergies that could be fractionations of any of the unaffected-arm synergies, accomplished by swapping the roles of the unimpaired- and impaired-arm synergies in the merging model described above (Eq. **S2**). Thus, in our model of synergy fractionation,

$$\vec{w}_k^{\,u} \approx \sum_{i=1}^{N^a} f_i^k \vec{w}_i^{\,a}, \quad f_i^k \geq 0, \quad k = 1...N^u, \qquad \textbf{[S3]}$$

where the coefficients $\vec{f}^{\,k} = [f_1^k, f_2^k, ..., f_{N^a}^k]$ specify how the kth unaffected-arm synergy may be fractionated into multiple synergies observed in the affected arm. As in the synergy-merging model, $\vec{f}^{\,k}$ was identified using nonnegative least squares. Because each affected-arm synergy could not simultaneously be fractionations of more than one unaffected-arm synergy, we imposed the additional constraint in the least-squares optimization that each affected-arm synergy could contribute to the reconstruction of at most one unaffected-arm synergy. This constrained optimization was accomplished by first performing the projection without any constraint. Then, for every affected-arm synergy, we identified the one unaffected-arm synergy with the highest associated coefficient, and this unaffected-arm synergy would be the only one whose reconstruction the affected synergy in question could contribute to. A second projection for every unaffected-arm synergy was then performed, this time only onto the affected-arm synergy(ies) assigned to it. An affected-arm synergy was defined to be a fractionation only if the $\vec{f}^{\,k}$'s identified indicated that it could be combined with another affected-arm synergy to reconstruct one of the unaffected-arm synergies.

We have found that the majority of the affected-arm muscle synergies identified as fractionations could neither be well matched directly to any unaffected-arm synergy nor be well reconstructed as a merging. However, in the case when an affected-arm synergy appeared to be similarly well explained as a merging or a fractionation, we assigned the synergy to whichever pattern gave a higher scalar product for the reconstruction.

Clustering Muscle Synergies. The unaffected-arm muscle synergies obtained from all subjects were categorized into classes to allow detection of the combinations of unaffected-arm synergies that tended to merge in the stroke-affected arm more frequently than others across subjects. Clustering was performed using the Matlab statistics-toolbox functions pdist (Minkowski option, $P = 3$), linkage (Ward option), and cluster.

1. Cheung VCK, et al. (2009) Stability of muscle synergies for voluntary actions after cortical stroke in humans. *Proc Natl Acad Sci USA* 106:19563–19568.
2. Delagi EF, Perotto A, Iazzetti J, Morrison D (1994) *Anatomical Guide for the Electromyographer* (Thomas, Springfield, IL).
3. Torres-Oviedo G, Macpherson JM, Ting LH (2006) Muscle synergy organization is robust across a variety of postural perturbations. *J Neurophysiol* 96:1530–1546.
4. Cheung VCK, d'Avella A, Bizzi E (2009) Adjustments of motor pattern for load compensation via modulated activations of muscle synergies during natural behaviors. *J Neurophysiol* 101:1235–1257.
5. d'Avella A, Bizzi E (2005) Shared and specific muscle synergies in natural motor behaviors. *Proc Natl Acad Sci USA* 102:3076–3081.
6. Cheung VCK, d'Avella A, Tresch MC, Bizzi E (2005) Central and sensory contributions to the activation and organization of muscle synergies during natural motor behaviors. *J Neurosci* 25:6419–6434.
7. Lee DD, Seung HS (1999) Learning the parts of objects by non-negative matrix factorization. *Nature* 401:788–791.
8. Cheung VCK, Tresch M (2005) Non-negative matrix factorization algorithms modeling noise distributions within the exponential family. *Conf Proc IEEE Eng Med Biol Soc* 5: 4990–4993.
9. Clark DJ, Ting LH, Zajac FE, Neptune RR, Kautz SA (2010) Merging of healthy motor modules predicts reduced locomotor performance and muscle coordination complexity post-stroke. *J Neurophysiol* 103:844–857.

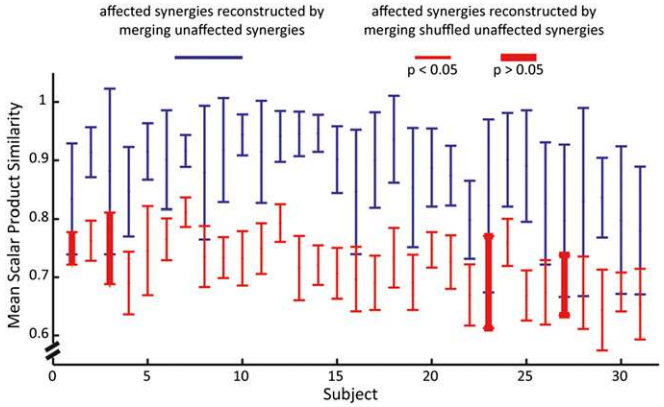

Fig. S1. The similarity between the extracted affected-arm synergies and their reconstructions through merging of unaffected synergies was statistically significant. To assess the goodness-of-fit of the synergy-merging model, we calculated the scalar-product values between the affected-arm synergies extracted from the EMGs and their reconstructions through merging of unaffected-arm synergies. For every subject (*x* axis), we averaged this scalar-product value across the affected-arm synergies (*y* axis, mean ± SD; blue). To assess the significance of these values, we compared them against baseline scalar-product values expected from chance (mean ± SD; red), obtained by comparing the original affected synergies with their reconstructions through merging of random synergies. The random synergies were generated by shuffling the muscle components of each of the original unaffected-arm synergies. For every affected-arm synergy, 100 trials of merging analysis were performed on random synergies, each time with a different shuffling, and an average scalar product was calculated across these 100 trials. As can be seen, for all subjects ($n = 31$), the original scalar-product values were higher than their corresponding baseline values, and for all but 4 subjects, this difference was statistically significant (*t* test, $P < 0.05$; thin red lines). Thus, the good agreement between the extracted and reconstructed affected-arm synergies is not a default result expected from the synergy-merging model per se.

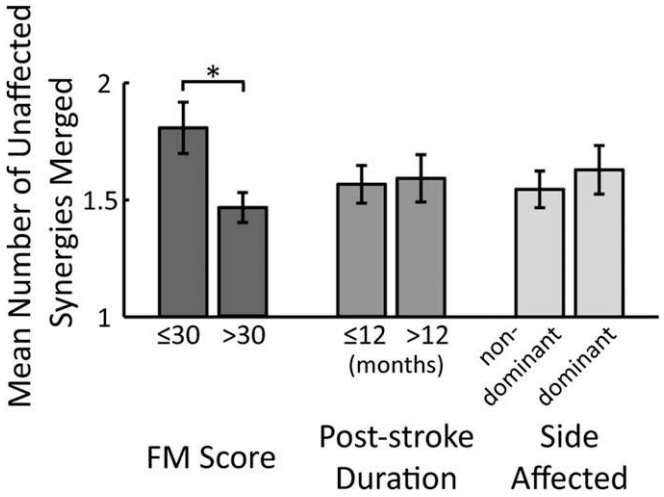

Fig. S2. The degree of muscle-synergy merging in the stroke-affected arm varied as a function of the degree of motor impairment, but not of the poststroke duration or of the side affected by stroke. To quantify the degree of muscle-synergy merging in the stroke-affected arm, for every subject we calculated the mean number of unaffected-arm synergies found merging into each affected-arm synergy as an index of the degree of merging. Thus, for this index, a value of 1 means no merging was observed. When calculating this average, we included in our statistics only those affected-arm synergies that could be well reconstructed (scalar product >0.75) as merging of unaffected-arm synergies. We found that this merging index (mean ± SE) was significantly higher in the severely impaired subject group [Fugl–Meyer scale (FM) ≤ 30, $n = 10$] than in the mildly to moderately impaired group (FM > 30, $n = 21$) [three-way ANOVA: $F(1, 30) = 8.0$, $^*P < 0.01$], but showed no difference between the acute (poststroke duration ≤12 mo, $n = 18$) and chronic (>12 mo, $n = 13$) groups ($F = 0.01$, $P > 0.9$) or between the groups affected on the nondominant ($n = 19$) and dominant ($n = 12$) sides ($F = 0.9$, $P > 0.3$).

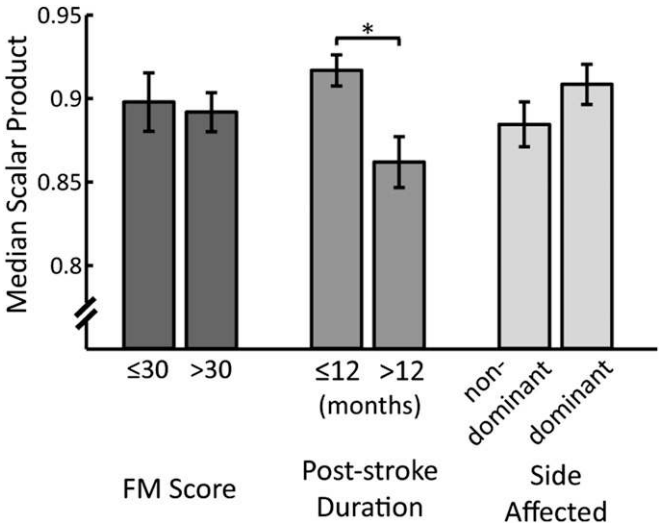

Fig. S3. The goodness-of-fit between the affected-arm muscle synergies and their reconstructions by merging unaffected-arm synergies was worse in patients with chronic stroke. For every patient, how well the affected-arm synergies could be reconstructed by linearly combining unaffected-arm synergies was quantified by the scalar product between the extracted and reconstructed synergies normalized to unit length, and the median scalar-product value was used as a goodness-of-fit measure for all subjects. We found that the median scalar product (mean ± SE) for the patients with chronic stroke (poststroke duration >12 mo) was significantly lower than that for the acute group (≤12 mo) [three-way ANOVA: $F(1, 30) = 9.8$, $^*P < 0.005$]. However, it showed no difference between the mildly impaired (FM > 30) and severely impaired (FM ≤ 30) groups ($F = 1.4$, $P > 0.2$) or between the groups affected on the nondominant and dominant sides ($F = 0.2$, $P > 0.6$). Thus, our model for explaining affected-arm synergies by merging unaffected-arm synergies was inadequate for the data obtained from patients with chronic stroke.

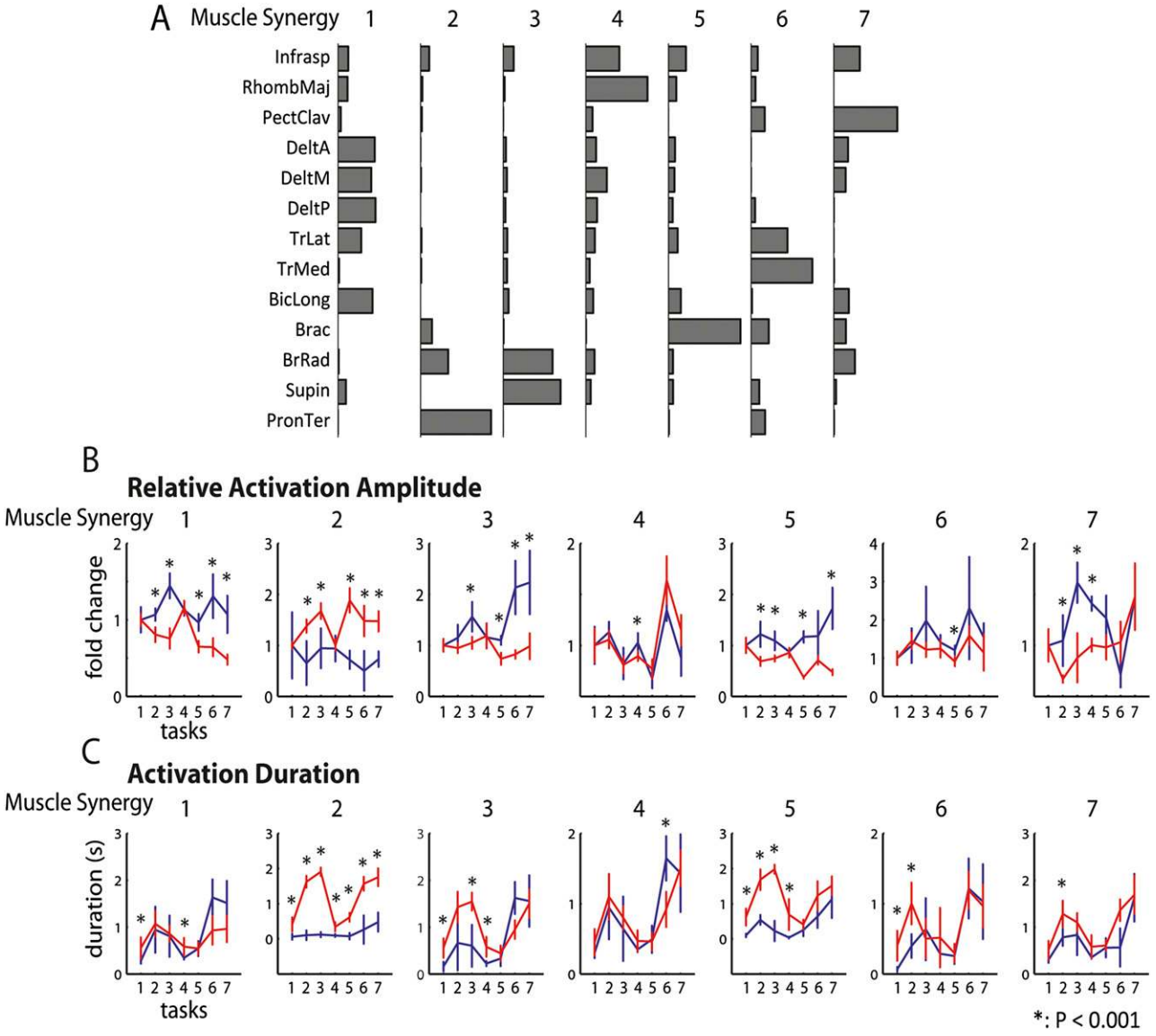

Fig. S4. Cortical stroke lesions changed the activation amplitude and duration of the coefficients of the preserved muscle synergies. We present analytic results of synergy coefficients from a mildly impaired patient (FM = 50) whose muscle synergies in the unaffected arm were preserved in the stroke-affected arm (Fig. 2*A*). (*A*) The preserved muscle synergies of this subject. In both arms, seven muscle synergies were required to achieve an EMG reconstruction R^2 of ~80%. We pooled the EMGs of the unaffected and stroke-affected arms together and reextracted muscle synergies (1–7) from this combined data matrix so that the we could compare the synergy coefficients of the two arms with respect to an identical set of basis vectors. The muscle synergies from this extraction were obviously very similar to the ones extracted separately from the EMGs of either arm (compare Fig. 2*A*). (*B*) To assess how the coefficient amplitude differed between the two arms, for each of the seven synergies we calculated the average coefficient amplitude of every trial across the data points exceeding 5% of the maximum coefficient amplitude. Because the EMGs of each arm were normalized values, an interarm amplitude comparison is possible only after the coefficient amplitude is standardized to a reference amplitude common to both arms. We accomplished this standardization by expressing, in both arms, the average amplitude of each task (tasks 2–7; mean ± SD; n = 10–11) as a fold-change deviation from the average amplitude of task 1. As can be seen, the relative coefficient amplitude of the stroke-affected arm (red) differed from that of the unaffected arm (blue) in a synergy- and task-specific manner. For instance, for synergy 3, the affected-arm amplitude was significantly smaller than the unaffected-arm amplitude only in tasks 3, 5, 6, and 7 (t test, $^*P < 0.001$); for synergy 4, on the other hand, the coefficient amplitude for the two arms was identical for all tasks except task 4. (*C*) The duration of activation of each synergy of the stroke-affected arm (red) was similarly compared with that of the unaffected arm (blue). They differed in a synergy- and task-specific manner, although in general the activation duration in the stroke-affected arm tended to be longer (e.g., in synergies 2, 3, and 5).

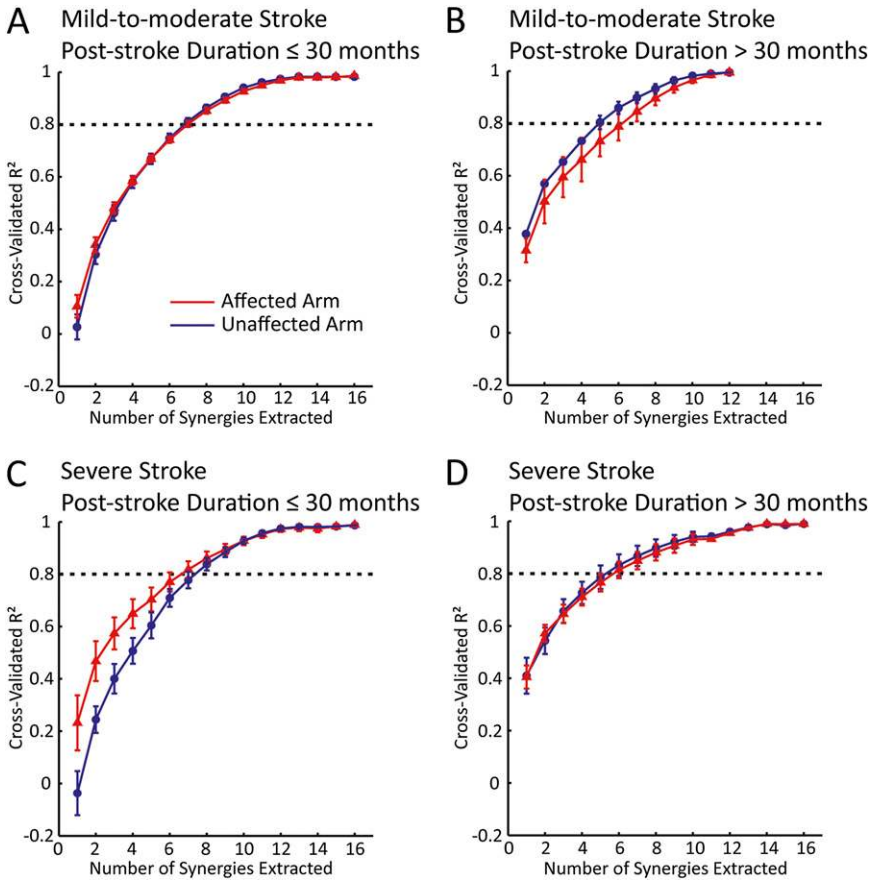

Fig. S5. EMG-data dimensionality in the stroke-affected arm decreased with more severe motor impairment, but increased with longer poststroke duration. In the data of each subject, the number of muscle synergies needed for adequate EMG reconstruction was determined by successively increasing the number of synergies extracted from one to the number of muscles recorded and then identifying the number at which an 80% of cross-validated R^2 (black dotted line) was achieved. We show here how the R^2 varied as a function of the number of synergies extracted in both the stroke-affected (red, mean ± SE) and the unaffected (blue) arms, in four nonoverlapping subject groups: subjects with mild-to-moderate motor impairment (FM > 30) (*A* and *B*), severe motor impairment (FM ≤ 30) (*C* and *D*), a ≤30-mo poststroke duration (*A* and *C*), and a >30-mo poststroke duration (*B* and *D*). An increase in the severity of motor impairment coincided with a left shifting of the stroke-affected R^2 curve relative to the unaffected-arm R^2 curve (compare *A* with *C* and *B* with *D*). This left-shifting of the R^2 curve suggests that fewer synergies were needed in the affected arm of severely impaired subjects for EMG reconstruction, consistent with the observation that the degree of synergy merging varied as a function of the degree of motor impairment (Fig. 3*B* and Fig. S2). On the other hand, an increase in the poststroke duration coincided with a right shifting of the stroke-affected R^2 curve relative to the unaffected-arm R^2 curve (compare *A* with *B* and *C* with *D*). This right-shifting of the R^2 curve indicates that more synergies were needed in the affected limb of very chronic stroke survivors for EMG reconstruction, consistent with the observation that the extent of synergy fractionation varied as a function of poststroke duration (Fig. 4*D*).

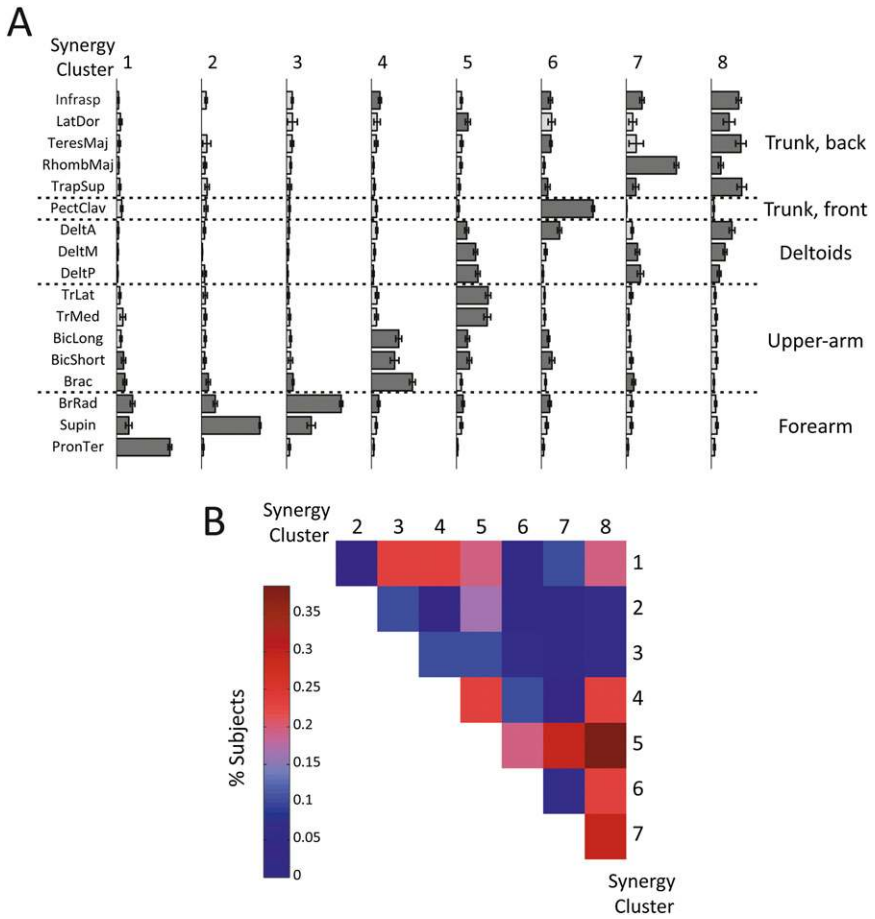

Fig. S6. Specific combinations of muscle synergies merged more frequently than others in the stroke-affected arm. (*A*) The muscle synergies of the unaffected arm across subjects. We grouped the unaffected-arm muscle synergies from all subjects into eight categories, using hierarchical clustering (*SI Materials and Methods*). Shown here are the averages (mean ± SE) of the synergy clusters (dark gray components, $P < 0.01$ and magnitude >0.1). (*B*) Heat map showing the frequency of occurrence of synergy merging in the stroke-affected arm, across all subjects, for all pairwise combinations of muscle synergies. The synergy clusters here (1–8) correspond to the ones shown in *A*. The frequency statistic reported for each combination includes instances of merging any number of synergies; thus, for example, the statistic for synergies 5 and 8 includes instances of merging just synergies 5 and 8, as well as instances of merging these two synergies plus another synergy. Note that some combinations of merging occurred much more frequently than others. In particular, synergy 8 (comprising mainly back muscles controlling the shoulder motion) merged frequently with synergies 4–7 (comprising muscles over both the elbow and the shoulder joints). The merging of these combinations of muscle synergies may account for previous observations of abnormal elbow–shoulder couplings in the paretic arm of stroke survivors. Note also that some merging combinations (e.g., merging of synergy 6 and synergy 1 or 2) were not observed in any patient.

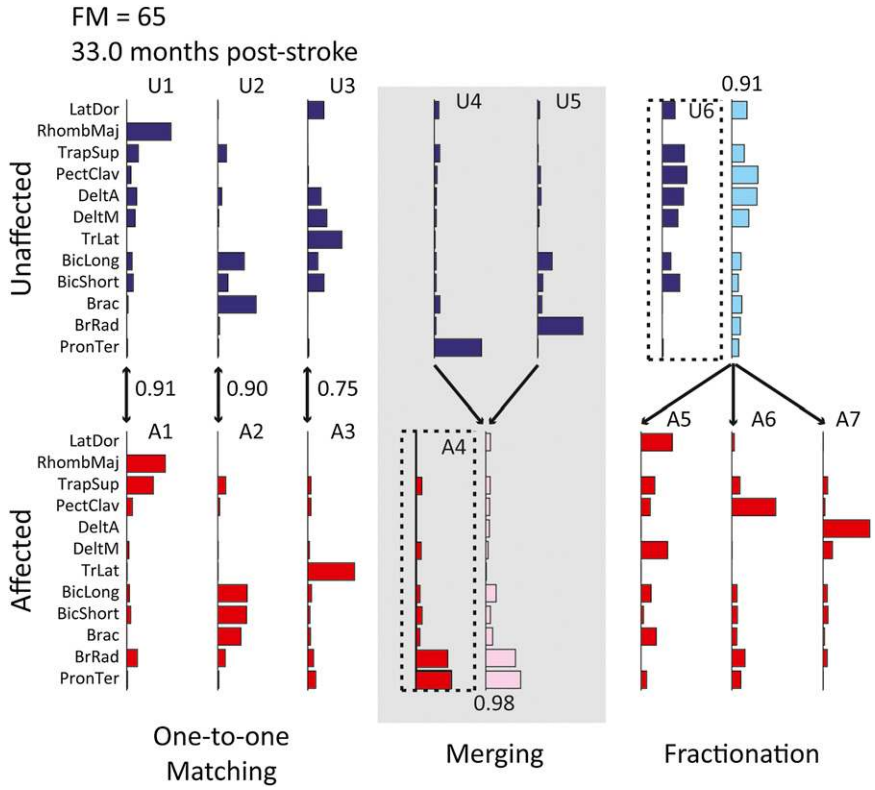

Fig. S7. Preservation, merging, and fractionation of muscle synergies in the stroke-affected arm of the same subject. We demonstrate here how the three patterns of muscle synergies we have described could be simultaneously present in the same subject. In this mildly impaired (FM = 65) and chronic (33.0 mo poststroke) survivor, six muscle synergies were identified for the unaffected arm (blue, *U1–U6*), and seven muscle synergies, for the stroke-affected arm (red, *A1–A7*). We found that one affected muscle synergy (*A4*) could be explained as a merging of two unaffected synergies (*U4* and *U5*) and be very well matched to its reconstruction (pink) via merging (scalar product of 0.98). Three affected synergies (*A5–A7*) were identified as fractionations of one unaffected synergy (*U6*), and together they could be linearly combined to reconstruct the fractionated unaffected synergy (cyan; scalar product of 0.91). The remaining affected-arm synergies unaccounted for by merging or fractionation (*A1–A3*) could each be matched to an unaffected synergy (*U1–U3*; scalar product of 0.75–0.91). Note that the three affected-arm synergies identified as fractionations (*A5–A7*) could be only very poorly reconstructed via merging (scalar product of 0.62–0.73), suggesting that merging and fractionation are two distinct, but complementary, patterns of muscle synergies in the stroke-affected arm.

Table S1. Summary of the stroke survivors recruited for this study

Subject	Sex	Age	FM score	Poststroke duration, mo	Side affected	No. muscles recorded	Lesion
1	F	59	58	8.5	D	12	Fronto-temporal: basal ganglia, internal capsule, insular
2	M	61	59	10.9	Nd	11	Fronto-temporo-parietal: M1, basal ganglia, insular
3	F	68	60	5.2	D	12	Fronto-parieto-occipital: M1, PMA, SMA
4	F	76	47	11.0	Nd	16	Fronto-temporal: M1, basal ganglia, internal capsule, insular
5	F	70	64	2.7	D	16	Fronto-temporo-parietal: M1, possibily PMA
6	M	57	18	14.7	Nd	12	Fronto-parietal: M1, PMA
7	F	46	29	17.5	Nd	14	Fronto-temporo-parietal: M1, with old lesions
8	M	44	64	2.0	Nd	13	Frontal: internal capsule, corona radiata, with old lesions
9	M	72	27	0.8	D	13	Fronto-temporo-parietal: M1, PMA, internal capsule, striatum, periventricular
10	F	75	50	2.1	Nd	13	Periventricular white matter
11	F	75	34	4.0	Nd	13	Fronto-temporo-parieto-occipital: M1, PMA, lenticular nucleus, cerebral white matter
12	F	51	0	1.6	D	12	Fronto-temporal: internal capsule, corticospinal tract, thalamus, pons, medulla oblongata
13	M	42	64	2.1	D	13	Fronto-parietal: focal ischemic lesion in parietal lobe
14	M	64	63	7.9	Nd	13	Fronto-temporal: M1, basal ganglia
15	M	58	66	0.9	D	13	Fronto-temporal: thalamus, lenticular nucleus
16	F	65	40	1.9	D	13	Fronto-temporal: lenticular nucleus, cerebral white matter
17	F	44	66	1.6	D	13	Fronto-temporal: M1, PMA, caudate nucleus, putamen, cerebral peduncle
18	M	72	25	4.5	Nd	13	Fronto-temporal: lenticular nucleus, cerebral peduncle
19	M	83	10	2.7	D	16	Fronto-temporal: thalamus
20	M	76	34	10.9	D	15	Parietal: postcentral gyrus
21	F	40	30	57.7	Nd	16	Fronto-temporo-parietal: M1, SMA, PMA
22	M	50	35	450.7	Nd	11	Corona radiata and basal ganglia lesions from hemorrhage
23	F	67	20	91.2	Nd	10	Frontal: basal ganglia
24	M	59	38	21.2	D	10	Fronto-temporo-parietal: M1, SMA, PMA
25	M	77	64	15.2	Nd	13	Fronto-temporo-parietal: bilateral subdural hematomas
26	F	69	66	23.1	Nd	13	Frontal: basal ganglia
27	F	46	65	33.0	Nd	13	Frontal: basal ganglia
28	M	60	41	13.0	Nd	14	Fronto-temporo-parietal: M1, SMA, PMA; contralateral occipital lobe
29	M	61	32	18.0	Nd	14	Fronto-temporal: M1, SMA
30	M	63	21	33.2	Nd	14	Fronto-temporal: postcentral gyrus and basal ganglia
31	M	60	16	263.6	Nd	14	Fronto-temporal lobes

D, dominant arm; Nd, nondominant arm; M1, primary motor cortex; PMA, premotor areas; SMA, supplementary motor cortex.